



# The exceptional photo-catalytic activity of ZnO/RGO composite via metal and oxygen vacancies

Ting-Ting Chen<sup>a</sup>, I-Chun Chang<sup>a</sup>, Min-Han Yang<sup>a</sup>, Hsin-Tien Chiu<sup>b</sup>, Chi-Young Lee<sup>a,\*</sup>

<sup>a</sup> Department of Materials Science and Engineering, National Tsing Hua University, Hsinchu 30013, Taiwan, ROC

<sup>b</sup> Department of Applied Chemistry, National Chiao Tung University, Hsinchu 30010, Taiwan, ROC

## ARTICLE INFO

### Article history:

Received 30 January 2013

Received in revised form 21 May 2013

Accepted 23 May 2013

Available online 31 May 2013

### Keywords:

Photocatalysis

Defect

Heterojunction

Graphene

ZnO

## ABSTRACT

ZnO/reduced graphene oxide (RGO) nanocomposite with many zinc and oxygen vacancies, synthesized in a simple solvothermal reaction exhibits significant photocatalytic activity. Photoluminescence and electron paramagnetic resonance measurements indicate that the zinc vacancies and oxygen vacancies were generated on the ZnO surface, and were crucial to that photocatalytic behavior. The photodegradation of methylene orange was significantly reduced by the addition of  $\text{h}^+$  and  $\cdot\text{OH}$  scavengers. Both zinc and oxygen vacancies cause effective charge separation in the photodegradation of methylene orange, which markedly inhibits the recombination of charges. The advanced photocatalytic behavior of the ZnO/RGO composite is discussed in detail herein.

© 2013 Elsevier B.V. All rights reserved.

## 1. Introduction

The design of highly efficient photocatalysts for the next generation is important. Not only must such photocatalysts have a large surface area, exposed faces and harvest light but also tailored defects and heterojunctions are typically introduced to enhance the photocatalytic performance [1–9]. The photoinduced rapid transfer of electrons to shallow defects or the junction level effectively minimizes charge recombination, markedly improving the performance of the heterostructure photocatalyst [10–23]. Heterostructures, such as noble metal/metal oxide, graphene/metal oxide, and hybrid metal oxide, have attracted much interest on account of their excellent photocatalytic performance, which follows from effective charge separation [8,9,24–41].

Among heterostructure photocatalysts, metal oxide/graphene nanocomposite is the one of greatest interest [8,24,25,28–30,32,34–38]. Graphene with carbon atoms packed in a hexagonal honeycomb two-dimensional structure has unique electrical properties, and acts as an excellent conductor [42]. Accordingly, the use of heterojunction materials of graphene and a suitable metal oxide is regarded as effective for charge separation in solar cells [25,34],

photoelectrochemical hydrogen production via water splitting [24,30,31,38], and photocatalysts [8,28,29,32,36,37].

Numerous recent studies have demonstrated that ZnO/graphene nanocomposite exhibits remarkable photocatalytic performance [28,29,32,37,43]. The close contact between the ZnO nanostructure and RGO is responsible for an electronic interaction that can promote charge separation. Under illumination, ZnO absorbs photon energy and produces electron–hole charge pairs. Graphene causes the charge pairs rapidly to separate and diffuse toward the surface before recombination: electrons rapidly transfer to graphene and holes simultaneously form highly reactive hydroxyl radicals. The improvement in the charge separation at the “real heterojunction” is considered to be the critical factor in highly efficient photocatalytic performance. Consequently, much research has focused on the synthesis of highly uniform nanocomposites with well dispersed ZnO on graphene sheet [37,44–49].

Photocatalytic activity can be enhanced by inducing tailored defects during synthesis. Zheng et al. [22] showed that different oxygen defects (oxygen vacancies and interstitial oxygen) that formed in a solvothermal process had an impact on the photocatalytic activity of ZnO. Dai and co-workers [19] developed enhanced the visible light photocatalytic activity of ZnO by narrowing the band gap with defects. Sun and co-workers [50] demonstrated that crystal defects in the ZnO layer changed the PL spectrum of the heterojunction ZnO–CuO composite. Zheng et al. [23] prepared an Ag/ZnO nanocomposite and found that its photocatalytic property is closely related to not only to the heterostructure but also to the

\* Corresponding author at: Department of Materials Science and Engineering, National Tsing Hua University, 101, Sec. 2, Kuang-Fu Road, Hsinchu 30013, Taiwan, ROC. Tel.: +886 3 5728692; fax: +886 3 5722366.

E-mail address: [cylee@mx.nthu.edu.tw](mailto:cylee@mx.nthu.edu.tw) (C.-Y. Lee).

oxygen defects. In spite of the above, early studies of ZnO/graphene have not considered the presence of defects. The formation of defects during the synthesis of ZnO/graphene must be considered, and the influence of defects on photocatalytic activity should be clarified.

Defects, heterojunctions, the absorption of pollutant on graphene, and the absorption of visible light are all potential candidates as the key factor in the enhancement of the photocatalytic performance of a ZnO/graphene system. In this study, a ZnO/reduced graphene oxide (RGO) composite was prepared in the solvothermal process. The photoluminescence (PL), electron paramagnetic resonance (EPR) and photocatalytic properties of samples are systematically investigated and discussed in detail. To clarify the effect of defects, the photocatalytic behaviors of ZnO/RGO with reactive species scavengers were examined.

## 2. Experimental

### 2.1. Materials preparation

In a typical solvothermal process, zinc acetate dihydrate and graphene oxide (GO) are used as precursors of ZnO and RGO, respectively, and ethanol acts as a reducing agent in a strong NaOH solution, which is utilized for the following two reasons; (1) to remove the functional groups from GO, which would inhibit the growth of the heterostructure of ZnO/RGO sheets, and to separate ZnO from RGO [37], and (2) to convert  $Zn^{2+}$  into ZnO.

All chemicals were analytical-grade reagents and used without further purification. Graphene oxide was prepared from commercial graphite by modified Hummers' method [51]. The concentration of GO suspension (pH 2.8) was about 1000 ppm. The ZnO/RGO nanocomposite was synthesized in a simple solvothermal reaction. In this typical experiment, 20 ml of 0.2 M NaOH in alcohol (99.5%) solution was freshly prepared. Further 0  $\mu$ l, 75  $\mu$ l, 100  $\mu$ l, and 150  $\mu$ l of GO suspension were injected into the NaOH solution respectively. Finally, 0.217 g zinc acetate dihydrate (0.05 M) was added into the each reaction solution. This solution mixture was further transferred to a 50 ml Teflon-lined stainless steel autoclave. The sealed autoclave was heated in an oven at 180 °C for 15 h, and then cooled down to room temperature slowly. After the solvothermal reaction, the white powder in the solution was collected by filtering, being washed and dried in an oven at 50 °C and thus obtained products were named as Z1, ZG75, ZG100, and ZG150 respectively.

### 2.2. Characterization

The morphology of the powder was investigated using a field emission scanning electron microscope (FE-SEM, Joel-6500, 15 kV) and a transmission electron microscope (TEM, JEM-2010, 200 kV). The crystal structure of the samples was characterized by powder X-ray diffraction (Bruker D8-advanced with Cu K $\alpha$  radiation  $\lambda = 1.5405981 \text{ \AA}$ ). X-ray photoelectron spectroscopy (XPS) was conducted on a PHI Quantera Spectrometer (ULVAC-PHI). The reflectance absorption spectrum of the powder was recorded on a UV/vis spectrometer (Avantes). Electron paramagnetic resonance (EPR) measurements were made at 77 K using a BRUKER X-band EPR spectrometer and a Xe lamp (XBO R 101W, OSRAM) was used as the light source. The mass ratio of RGO in ZnO/RGO was calculated from the weight loss of 250–700 °C in the TGA analysis (PerkinElmer thermal analysis TG/DTA system) and shown in the supporting information. The RGO contents in ZG75, ZG100, and ZG150 are 2.0 wt%, 1.6 wt%, and 1.2 wt%, respectively.

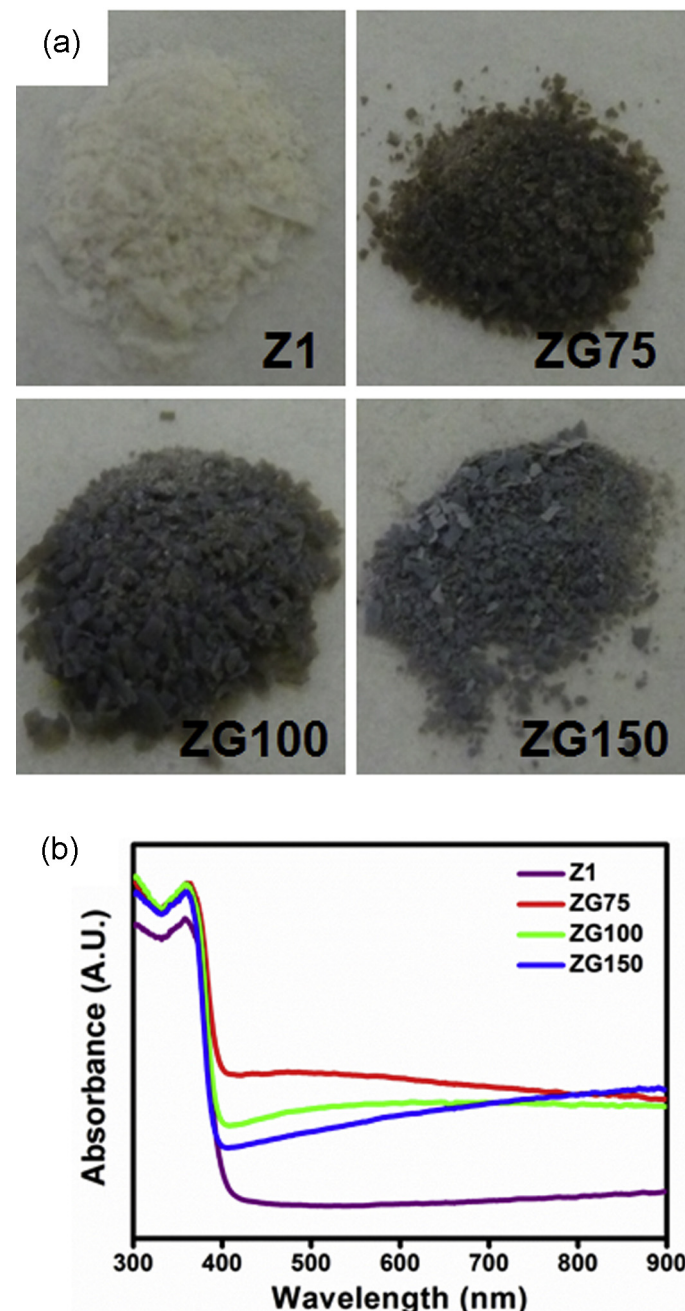


**Fig. 1.** (a) Photograph and (b) reflectance absorption spectrum of as-synthesized samples.

### 2.3. Photocatalytic test

According to the literature [41], the photodegradation of MO is a pseudo-first-order reaction and its kinetics can be expressed as  $\ln(C_0/C_t) = kt$ , where  $k$  is the apparent rate constant, and  $C_0$  and  $C_t$  are the concentrations of MO at initial state and after illumination for  $t$  min, respectively. The photocatalytic tests comprised two parts.

#### 2.3.1. Photocatalytic test under a wide range of irradiation (from UV to visible light) with and without charge scavenger

In the first part, all tests were carried out using a 180 W Xe lamp (XBO 180 W, OSRAM) which includes both UV light and visible light. As is typical, 10 mg of powder was dispersed into an aqueous solution of 17 ppm MO. Before irradiation, the suspension was magnetic stirred in the dark for 5 min to establish the

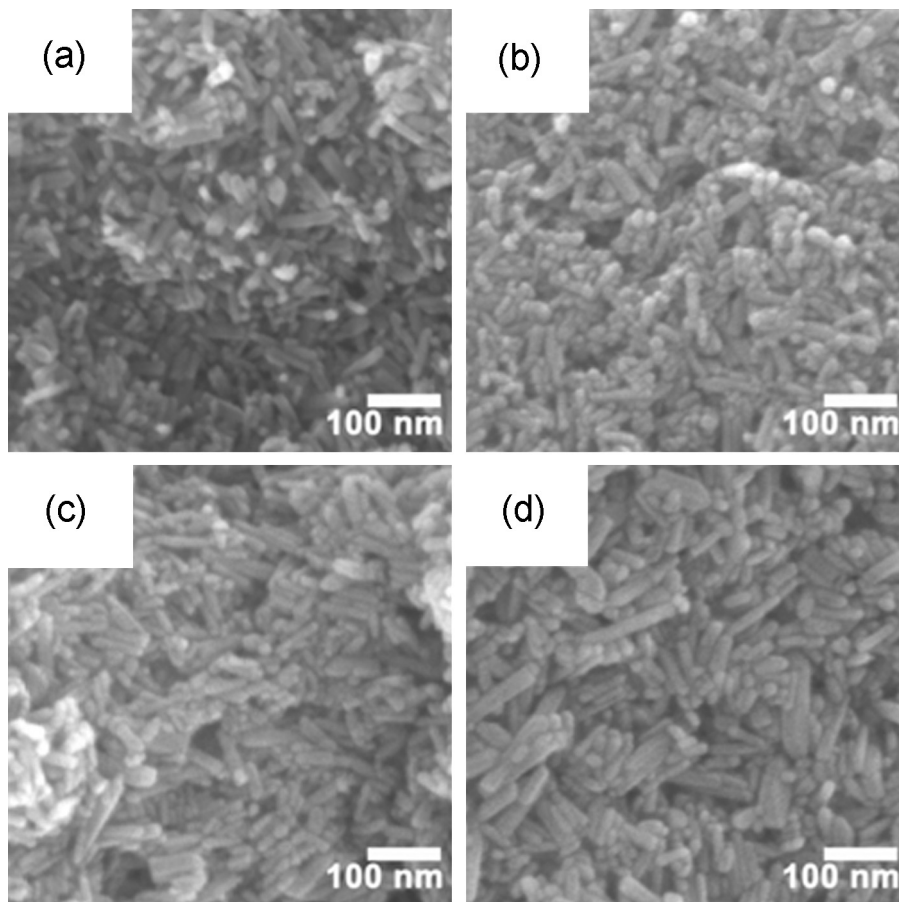


**Fig. 2.** FE-SEM images of pure ZnO and ZnO/RGO composite (a) Z1; (b) ZG75; (c); ZG100; (d) ZG150.

absorption–desorption equilibrium. Under illumination, 1 ml of solution was injected out at the given time intervals, which was further analyzed by recording the absorption at 435 nm using a UV/vis spectrometer (Avantes).

The tests with scavenger were carried out under the same experimental conditions as above, whereas the specific charge scavenger was added into the suspension before stirring. Here, Sodium oxalate [52,53], H<sub>2</sub>O<sub>2</sub> [54], ethanol [32,53], and ascorbic acid [55] were used as scavengers of hole, hydroxyl radical, and oxygen radical, respectively. Afterwards, the experimental process was carried out as described above. The participation of these reactive species in the photodegradation can be identified with assistance of the scavenger which will withdraw the corresponding reactive species and cause a decrease of photoactivity. The change of photodegradation rate constant can be related to the role of the reactive species [52–54].

### 2.3.2. Photocatalytic test under visible light only

In the second part, all tests were carried out under a 101 W Xe lamp (XBO R 101 W, OSRAM) that was equipped with a 420 nm filter. Generally, 10 mg of powder was dispersed into an aqueous solution of 8 ppm MO. Afterwards, the experimental process was carried out as described above.

## 3. Results and discussion

**Fig. 1a** displays photographs of the as-synthesized samples. Zinc oxide with a 3.2 eV band edge, Z1, has a pearl-like appearance, as reported in the literature. ZnO/RGO varied from dark to light purple as the carbon content in the samples increased. The absorption

spectrum, shown in **Fig. 1b**, indicates that all samples had the same absorption band edges (ca. 3.2 eV) but clearly different the band tails in the visible and infrared range. ZG75 had a descending band tail and was between deep purple and dark brown; ZG100 had a horizontal band tail and was deep purple, and ZG150 had an ascending band tail and was light purple. According to literature report, RGO and defects are responsible for the absorption of light with energies below the band gap of metal oxide [11,29,32,56,57,19]. The types of defects in ZnO/RGO was subsequently investigated in further detail using electron paramagnetic resonance (EPR).

### 3.1. Characterization of as-synthesized ZnO/RGO

The SEM images in **Fig. 2a** show nanorods (Z1) with a width of ca. 10–40 nm and a length of around 20–120 nm, which were obtained in the solvothermal reaction at 180 °C without the addition of GO suspension. **Fig. 2b–d** present SEM images of the as-synthesized samples that were obtained with the addition of 75, 100 and 150 µl GO suspension, respectively. They clearly demonstrate that the width and length of the ZnO rods both increased with the amount of GO suspension. EDS analysis yields the C, O, and Zn signals from the as-synthesized samples, as indicated in the supporting information. The presence of the C peak is attributable to RGO and contamination that was caused by the exposure of the samples to air. According to the TGA analysis, the RGO mass ratios of the three ZnO/RGO composites are 1.2–2.0%, which are calculated from the weight loss from 250 to 700 °C (see Supporting Information Fig. S1).

The crystalline structure of the samples was characterized by powder X-ray diffraction (XRD). The XRD diffraction patterns in **Fig. 3** reveal that all of the as-synthesized samples, Z1 and ZG100,

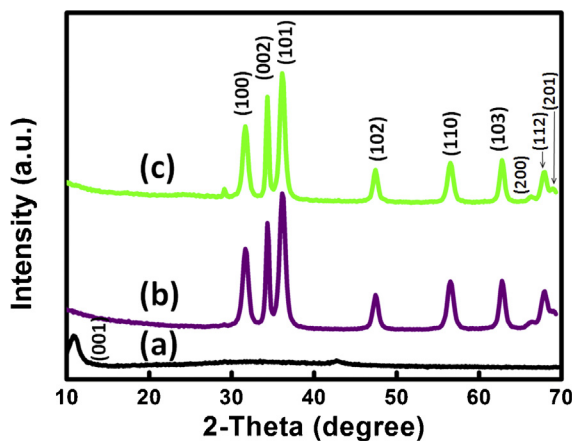


**Fig. 3.** XRD pattern of as-synthesized samples: (a) GO; (b) Z1; (c) ZG100.

are crystalline with characteristic diffraction peaks at  $31.7^\circ$ ,  $34.4^\circ$  and  $36.2^\circ$ , which correspond to the wurtzite phase (JCPDS 36-1451) and indexed as (100), (002) and (101), respectively. Neither the diffraction peak assigned to GO at  $11^\circ$  nor that assigned to RGO at  $26^\circ$  was observed.

X-ray photoelectron spectroscopy (XPS) was applied to examine the chemical environment of each element, Zn, O and C, in the composite, as presented in Fig. 4. In Fig. 4a, the C 1s spectrum of GO was deconvoluted into three peaks at 284.5, 286.7 and 288.2 eV, which were assigned to C–C, C–OH and C=O, and O=C–OR, respectively [29,35,37,44]. The strength of the peaks that were assigned to C–OH and C=O indicated the high degree of oxidation of the GO. The C 1s spectrum of ZG100 (Fig. 4b) shows a significant lower peak at 285.5 eV, which was assigned to C–OH and C=O. The decrease in the oxygen content shows that GO was reduced to RGO in a basic solution of ethanol, as has been reported earlier [58]. Notably, the higher content of O=C–OR in ZG100 than in GO may be attributable to the adsorption of O=C–OR during

the hydrolysis of the zinc acetate dihydrate [37]. The O 1s spectra of both Z1 and ZG100 comprised three peaks which centered at 529.7, 530.5, and 531.6 eV, as displayed in Fig. 4c. The peak centered at a high binding energy of 531.6 eV is usually associated with the chemisorbed oxygen on the surface of ZnO. The peak at a low binding energy of 529.7 eV is attributed to  $O^{2-}$  ion in the wurtzite lattice. The middle peak at 530.5 eV is associated with the  $O^{2-}$  ion that is located in an imperfect wurtzite lattice with oxygen deficiencies [19,59]. This result suggests that the oxygen vacancies were formed on the ZnO nanorod surface during the solvothermal process. Fig. 4d shows that the  $Zn2p_{3/2}$  peaks of both Z1 and ZG100 are centered at 1021.1 eV. The absence of an observed shift in the  $Zn2p_{3/2}$  peak from ZG100 indicates the lack of any effect of the chemical environment on the GO-assisted synthesis of ZnO, which reveals the non-existence of an electronic interaction between ZnO and RGO in the as-synthesized ZG100 [37,60].

### 3.2. EPR investigations of ZnO/RGO

EPR spectroscopy was utilized to investigate the defects in ZnO/RGO nanocomposites with and without illumination, as shown in Fig. 5a. Based on the literature, the signals at  $g = 1.987$  and 2.021 were attributed to the oxygen interstitials [61–63], and chemisorbed oxygen on the surface of ZnO/RGO [61,64], respectively. Two more signals at  $g = 1.958$  and 2.003 were also observed. The origin of these EPR features is still highly controversial. For example, several hypotheses have been proposed to explain the signal at  $g \sim 1.96$ , involving, such as, oxygen vacancies [63,65–68], free electrons [69,70], and shallow donors [16,71–73]. Zheng et al. [22] reported that oxygen vacancies formed on the surface of ZnO nanorods in the solvothermal process when ethanol was used as a reducing agent. Under the experimental conditions herein, which were similar to those in the study of Zheng, the paramagnetic signal at  $g = 1.958$  was considered to be associated with a single positive charged oxygen vacancy ( $V_O^+$ ) [63,65–68], and the signal at  $g = 2.003$  was attributed to a single negative charged zinc vacancy

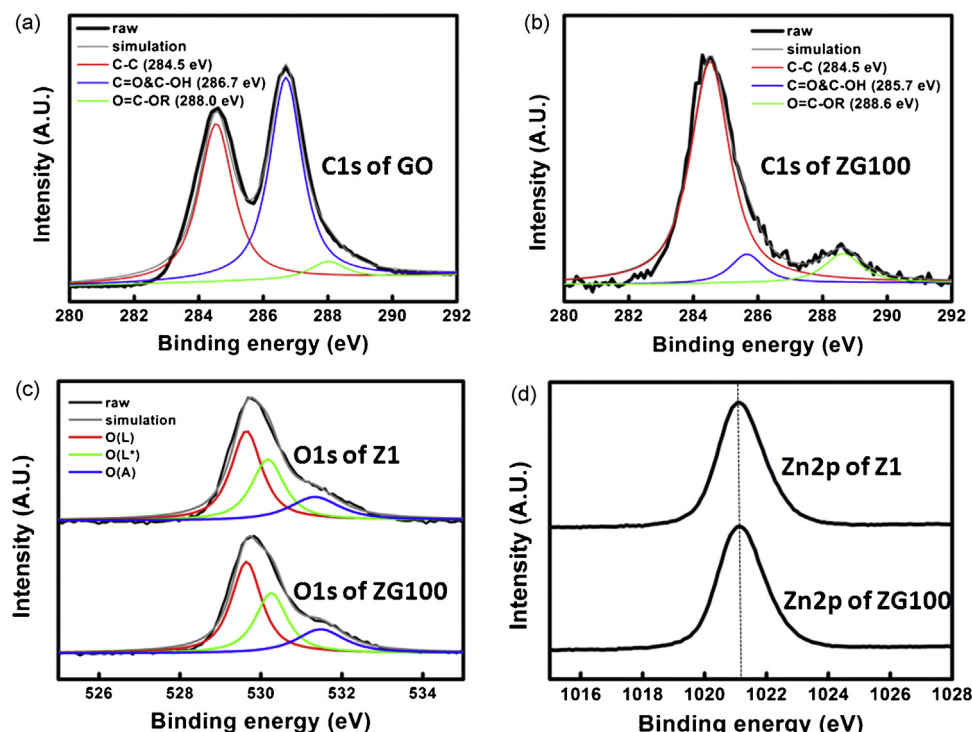


**Fig. 4.** C 1s XPS spectra of (a) GO and (b) ZG100; (c) O 1s and (d)  $Zn2p_{3/2}$  XPS spectra of Z1 and ZG100.

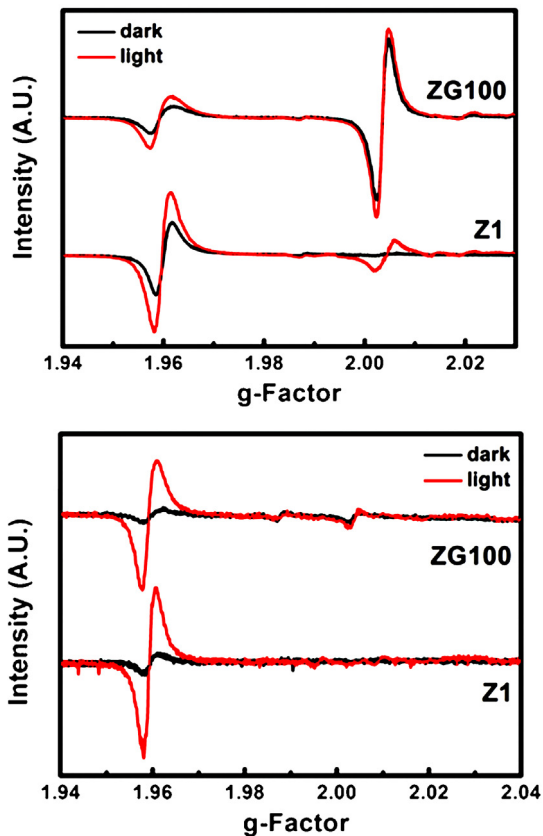


**Fig. 5.** EPR spectra of (a) powder and (b) suspensions of Z1 and ZG100 at 77 K.

( $V_{\text{Zn}}^-$ ) [61–63,74]. As presented in Fig. 5a, the EPR spectrum of Z1 includes a stronger signal at  $g = 1.958$  and a light-induced signal at  $g = 2.003$ . Compared with Z1, the EPR spectrum of ZG100 powder shows a very strong signal at  $g = 2.003$ , even in the absence of illumination, whereas the peak intensity at  $g = 1.958$  is less in the presence of illumination. Typically, an EPR spectrum reveals different defects in metal oxide, such as vacancies and interstitials.

Unlike Z1, ZG100 contained not only donor-type oxygen vacancies but also acceptor-type zinc vacancies. Zinc vacancies in ZnO generate partially occupied states that were close to the valence band [75]. The partially filled states accepted additional electrons from the conduction band, resulting in luminescence around 2.75 eV (450 nm), which value is highly consistent with the observed transition energy of ZG100, as described in the supporting information (Fig. S2). The strong EPR signal at  $g = 2.003$  and the emission peak at  $\sim 450$  nm in the PL spectra of ZnO/RGO suggest that zinc vacancies were formed in the GO-assisted solvothermal reaction. The EPR signal at  $g = 1.958$ , which is related to the formation of oxygen vacancies results from a local level near the conduction band [18,68,75]. The emission peaks at around 480 nm were obtained from both Z1 and ZG100 and could be assigned to oxygen vacancies ( $V_O^+$ ,  $V_O^{++}$ ).

### 3.3. Photocatalytic test

The outstanding photocatalytic activity of various ZnO/RGOs was examined by the photodegradation of 17 ppm methyl orange (MO), illuminated under a 180 W Xe lamp, whose spectrum contained both UV and visible light, as shown in Fig. 6. Z1 and ZnO/RGO nanocomposites (ZG75, ZG100, and ZG150) exhibited better photocatalytic performance than the commercial photocatalyst TiO<sub>2</sub> (P25, Degussa). In particular, the rate constant for the degradation

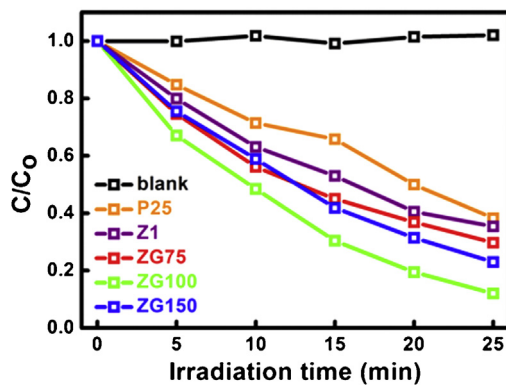


**Fig. 6.** Photodegradation of MO by P25, pure ZnO (Z1), and ZnO/RGO (ZG75, ZG100, and ZG150) under UV-vis light irradiation.

of MO by ZG100 ( $0.0844 \text{ min}^{-1}$ ) is more than double those of P25 ( $0.0370 \text{ min}^{-1}$ ) and Z1 ( $0.0423 \text{ min}^{-1}$ ), as presented in Table 1.

The photocatalysis of a photoreaction using a semiconductor material as a catalyst includes the following four steps [1,2,5–7]. (1) The semiconductor absorbs photon energy ( $h\nu \geq E_g$ ) and generates electron–hole charge pairs; (2) the charges are separated and diffuse toward the surface before recombination; (3) electrons in the conduction band are transferred to adsorbate O<sub>2</sub> molecules and super oxide radicals (O<sub>2</sub><sup>•-</sup>) are produced; (4) holes in the valence band directly oxidize the organic pollutant or form extremely powerful hydroxyl radicals (•OH) by interfacial charge transfer. Therefore, the generation of charge pairs, the separation of the charges, and the activation of the reactive species are all important processes in photocatalysis.

In this work, both ZG100 and Z1 were inactive under illumination of visible-light using a Xe lamp with a 420 nm long-pass filter. This result indicates that generation of charges in the visible light range was insensitive for Z1. In addition, ZG100 was also inactive even though it absorbs the light above 420 nm in the absorption spectrum owing to the existence of defects and RGO. Even though the carbon-related material is known to be a good dye adsorbent [36,76,77], the TGA analysis and dye adsorption test exclude the absorption of dye by graphene as a cause of the enhancement of photocatalytic performance, as presented in the supporting information (Fig. S3). Here, the enhancement of photocatalytic activity by crystal defects and the heterojunction between the RGO and ZnO are further investigated.

### 3.4. Defects

As reported elsewhere [6,8,10,11,13–15,17–23,46], defects in ZnO strongly influence the photocatalytic activity. EPR measurements of dispersed ZG100 and Z1 (~75,000 ppm, in DI water) were further performed with and without illumination at 77 K, as shown in Fig. 5b. The intensity of the peaks from both ZG100 and Z1 at  $g = 1.958$ , assigned to oxygen vacancies, increased upon illumination, and the increase in intensity was particularly large for Z1. However, the signals at  $g = 1.988$  and 2.003, attributed to oxygen interstitial and zinc vacancies, respectively, were obtained only from ZG100. According to these observations and the EPR results for Z1 and ZG100 powders, ZG100 with both donor ( $V_O^-$ ) and acceptor ( $V_{\text{Zn}}^-$ ) vacancies exhibited excellent photoactivity. Fig. 7 displays the proposed band structure and charge-transfer process of the photocatalyst. Two defect states, oxygen vacancies and zinc vacancies, act as charge traps. The  $V_{\text{Zn}}$  acceptor level close to the valence band can trap the holes and  $V_O$  donors near the conduction band can trap the electrons. Consequently, the rapid charge separation efficiently prevents the recombination of electrons and holes. Unlike

**Table 1**

Photodegradation rate constant ( $\text{min}^{-1}$ ) of ZG100 and Z1 with assistance of different scavengers.

	MO only	AA <sup>a</sup> ( $\text{O}_2^{\bullet-}$ )	Ethanol <sup>b</sup> ( $\bullet\text{OH}_b$ )	$\text{Na}_2\text{C}_2\text{O}_4^c$ ( $\text{h}^+$ )	$\text{H}_2\text{O}_2^d$ ( $\text{h}^+, \bullet\text{OH}_s$ )
Z1	0.0423	0.0328	0.0056	0.0478	0.0304
ZG100	0.0844	0.0692	0.0117	0.0622	0.0315

<sup>a</sup> Ascorbic acid (AA) was served as a scavenger of  $\text{O}_2^{\bullet-}$ .

<sup>b</sup> Ethanol was served as a scavenger of  $\bullet\text{OH}_b$ .

<sup>c</sup>  $\text{Na}_2\text{C}_2\text{O}_4$  was served as a scavenger of  $\text{h}^+$ .

<sup>d</sup>  $\text{H}_2\text{O}_2$  was served as scavengers of  $\text{h}^+$  and  $\bullet\text{OH}_s$ .

ZG100, Z1 with oxygen vacancies traps electrons only, and so cannot separate the charges. Hence, recombination is not effectively prevented.

To investigate further the proposed photocatalytic mechanism for ZG100 and Z1, charge scavengers were used in the photocatalytic reactions. As is generally known, photo-generated holes transformed to  $\bullet\text{OH}_s$  ( $\bullet\text{OH}$  bound to the catalyst surface),  $\bullet\text{OH}_b$  ( $\bullet\text{OH}$  in the bulk solution), and electrons transformed to  $\text{O}_2^{\bullet-}$ , which will react with organic pollutants. Holes can be also regarded as a potential reactive species that can oxidize organic pollutants [6,53]. According to the literature, sodium oxalate scavenges  $\text{h}^+$ ; [52,53] highly concentrated  $\text{H}_2\text{O}_2$  scavenges  $\text{h}^+$  and  $\bullet\text{OH}_s$ ; [54] ethanol scavenges  $\bullet\text{OH}_b$  [32,53], and ascorbic acid scavenges  $\text{O}_2^{\bullet-}$  [55]. Fig. 8 and Table 1 show the photocatalytic performance obtained with different scavengers. When ethanol was added to capture  $\bullet\text{OH}_b$ , the rate constants of both Z1 and ZG100 photocatalytic reactions considerably declined, suggesting that  $\bullet\text{OH}_b$  is the major active species in those cases. The addition of 0.1  $\mu\text{mol}$  ascorbic acid as an  $\text{O}_2^{\bullet-}$  scavenger reduced the photodegradation rate constants of Z1 and ZG100 by 21% and 18%, respectively. The rate constant of ZG100 was still double than that of Z1, revealing that  $\text{O}_2^{\bullet-}$  cannot be used to differentiate between Z1 and ZG100. However, adding 0.1  $\mu\text{mol}$   $\text{Na}_2\text{C}_2\text{O}_4$  as an  $\text{h}^+$  scavenger reduced the photodegradation rate constant of ZG100 by 26%, but did not affect the rate constant of Z1. This observation strongly suggests that direct oxidation by separated holes on the ZG100 surface is an additional reaction pathway. Furthermore, when highly concentrated  $\text{H}_2\text{O}_2$  was used to scavenge  $\text{h}^+$  and  $\bullet\text{OH}_s$ , the photodegradation was mainly attributed to the photo-induced electrons. Under this condition, the photodegradation rate constants of both ZG100 (0.0315  $\text{min}^{-1}$ , 63% reduced) and Z1 (0.0304  $\text{min}^{-1}$ , 29% reduced)

were decreased and almost equal, which implies that the same amount of electrons were photoinduced in Z1 and ZG100. The results of the photocatalytic test with different scavengers were consistent with the EPR analysis. The excellent photoactivity of ZG100 arises from both zinc and oxygen vacancies, which trap holes and electrons, respectively, whereas Z1 with oxygen vacancies exhibits only a fairly good performance.

### 3.5. Heterojunction in MO solution

In previous investigations, the outstanding photocatalytic activity of ZnO/RGO composite was attributed mainly to the charge separation that results from the heterojunction between ZnO and RGO [8,24–26,28–30,32–38,77]. In the as-synthesized ZG100, ZnO and RGO are separated, according to TEM observation, as described in the supporting information (Fig. S4). Additionally, according to XPS analysis, the binding energies of  $\text{Zn}2\text{p}_{3/2}$  in ZnO (Z1) and ZnO/RGO composite (ZG100) are same, suggesting the absence of bonding between ZnO and RGO. However, based on our earlier work [78], two materials with matching band positions can be transformed into a “visionary heterostructure” in the solution owing to the electrostatic adsorption. This attraction can dominate the interaction and contribute to the inter-particle bonding, promoting the transfer of electrons between particles and thereby increasing photocatalytic activity. According to earlier studies [8,29,32,34–36], the flat band potential of ZnO is higher than that of RGO, indicating that electrons in ZnO can flow toward graphene. The zeta potential of Z1, ZG100, and RGO in solution at pH 8 (the test MO solution at pH 8) were +25.8, +23.5, and −36.6, respectively. The positively charged RGO may have attracted negatively charged ZnO to form a “visionary ZnO/RGO heterostructure”. Fig. S5 shows the slightly

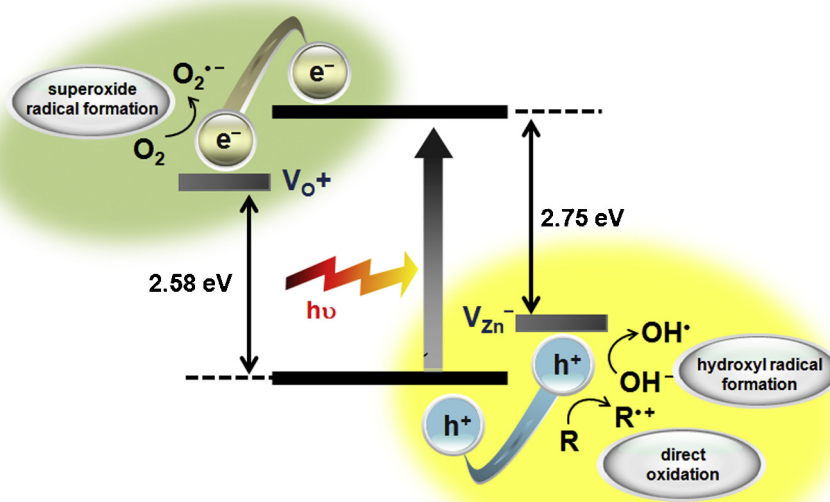


Fig. 7. Proposed band structure and charge-transfer process of ZG100 photocatalyst.

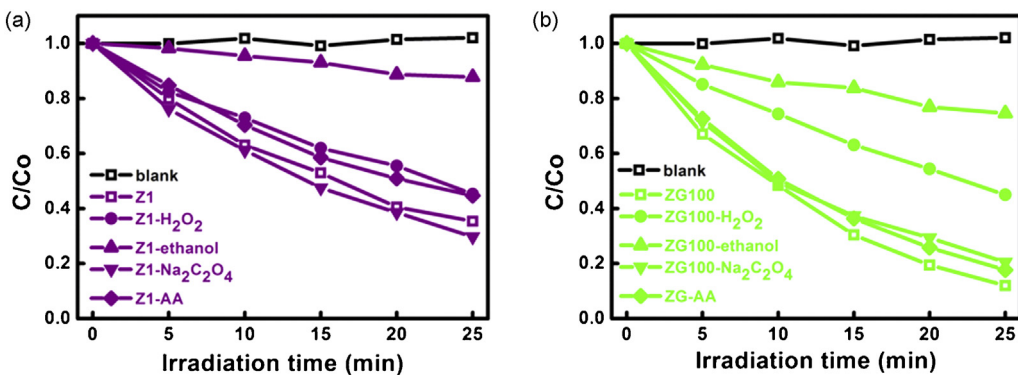


Fig. 8. Photodegradation of MO by (a) Z1 and (b) ZG100 with the assistance of scavengers.

enhanced photocatalytic performance of the simple mixture of Z1 and RGO, whose rate constant for MO degradation ( $0.051 \text{ min}^{-1}$ ) is larger than that of Z1 ( $0.042 \text{ min}^{-1}$ ). The TEM images of ZG100 and mixture of Z1 and RGO after photocatalytic test (see Supporting Information Fig. S6) include ZnO rods decorated on the RGO. The improved performance is attributable to the facilitation of electron transfer to RGO. Nevertheless, the comparison of the rate constants of ZG100 and the mixture demonstrate that the heterojunction is not essential to this process.

#### 4. Conclusions

In summary, a ZnO/RGO nanocomposite was successfully synthesized using GO and zinc acetate dihydrate in a solvothermal process. Zinc and oxygen vacancies in the ZnO/RGO nanocomposite exhibit excellent photocatalytic activity. The paramagnetic defects of zinc and oxygen vacancies, were identified in EPR experiments, which significantly enhance the photocatalytic activity of ZnO/RGO. The photo-induced charges, holes and electrons were trapped by  $V_{\text{Zn}}$  acceptor and  $V_{\text{O}}$  donor respectively. Furthermore, the scavenger-assisted photocatalytic reactions show that  $\text{h}^+$  and  $\cdot\text{OH}$  enhanced the photoactivity of ZG100 as the photocatalyst. The presence of both zinc and oxygen vacancies in ZG100 induced effective charge separation in the photodegradation process. In this case, other factors such as, heterojunction, the absorption of visible light, and the absorption of dye by graphene were negligible for the enhancement of photocatalytic performance of ZG100.

#### Acknowledgements

The authors would like to thank the National Science Council of the Republic of China, Taiwan, for financially supporting this research under Contract No. NSC 101-2113-M-007-012-MY3. Ted Knoy is appreciated for his editorial assistance.

#### Appendix A. Supplementary data

Supplementary data associated with this article can be found, in the online version, at <http://dx.doi.org/10.1016/j.apcatb.2013.05.059>.

#### References

- [1] D. Beydoun, R. Amal, G. Low, S. McEvoy, J. Nanopart. Res. 1 (1999) 439–458.
- [2] P.V. Kamat, J. Phys. Chem. Lett. 3 (2012) 663–672.
- [3] S. Liu, J. Yu, M. Jaroniec, J. Am. Chem. Soc. 132 (2010) 11914–11916.
- [4] A. McLaren, T. Valdes-Solis, G. Li, S.C. Tsang, J. Am. Chem. Soc. 131 (2009) 12540–12541.
- [5] N. Serpone, A.V. Emeline, J. Phys. Chem. Lett. 3 (2012) 673–677.
- [6] W.Y. Teoh, J.A. Scott, R. Amal, J. Phys. Chem. Lett. 3 (2012) 629–639.
- [7] H. Tong, S. Ouyang, Y. Bi, N. Umezawa, M. Oshikiri, J. Ye, Adv. Mater. 24 (2012) 229–251.
- [8] Q. Xiang, J. Yu, M. Jaroniec, Chem. Soc. Rev. 41 (2012) 782–796.
- [9] J. Yu, L. Qi, M. Jaroniec, J. Phys. Chem. C 114 (2010) 13118–13125.
- [10] S. Baruah, S.S. Sinha, B. Ghosh, S.K. Pal, A.K. Raychaudhuri, J. Dutta, J. Appl. Phys. 105 (2009) 074306–074308.
- [11] D.S. Bohle, C.J. Spina, J. Am. Chem. Soc. 131 (2009) 4397–4404.
- [12] A.W. Cohn, K.R. Kittilstved, D.R. Gamelin, J. Am. Chem. Soc. 134 (2012) 7937–7943.
- [13] M.Y. Guo, A.M.C. Ng, F. Liu, A.B. Djurišić, W.K. Chan, H. Su, K.S. Wong, J. Phys. Chem. C 115 (2011) 11095–11101.
- [14] M. Kong, Y. Li, X. Chen, T. Tian, P. Fang, F. Zheng, X. Zhao, J. Am. Chem. Soc. 133 (2011) 16414–16417.
- [15] Y. Lai, M. Meng, Y. Yu, X. Wang, T. Ding, Appl. Catal. B-Environ. 105 (2011) 335–345.
- [16] W.K. Liu, K.M. Whitaker, K.R. Kittilstved, D.R. Gamelin, J. Am. Chem. Soc. 128 (2006) 3910–3911.
- [17] R.M. Sheetz, E. Richter, A.N. Andriotis, M. Menon, Phys. Rev. B 80 (2009) 195314–1–195314–4.
- [18] J. Wang, P. Liu, X. Fu, Z. Li, W. Han, X. Wang, Langmuir 25 (2008) 1218–1223.
- [19] J. Wang, Z. Wang, B. Huang, Y. Ma, Y. Liu, X. Qin, X. Zhang, Y. Dai, ACS Appl. Mater. Interfaces 4 (2012) 4024–4030.
- [20] H. Zeng, W. Cai, P. Liu, X. Xu, H. Zhou, C. Klingshirn, H. Kalt, ACS Nano 2 (2008) 1661–1670.
- [21] Y. Zheng, C. Chen, Y. Zhan, X. Lin, Q. Zheng, K. Wei, J. Zhu, J. Phys. Chem. C 112 (2008) 10773–10777.
- [22] Y. Zheng, C. Chen, Y. Zhan, X. Lin, Q. Zheng, K. Wei, J. Zhu, Y. Zhu, Inorg. Chem. 46 (2007) 6675–6682.
- [23] Y. Zheng, L. Zheng, Y. Zhan, X. Lin, Q. Zheng, K. Wei, Inorg. Chem. 46 (2007) 6980–6986.
- [24] N.J. Bell, Y.H. Ng, A. Du, H. Coster, S.C. Smith, R. Amal, J. Phys. Chem. C 115 (2011) 6004–6009.
- [25] J. Chen, C. Li, G. Eda, Y. Zhang, W. Lei, M. Chhowalla, W.I. Milne, W.-Q. Deng, Chem. Commun. 47 (2011) 6084–6086.
- [26] Y. Huang, Y. Wei, J. Wu, C. Guo, M. Wang, S. Yin, T. Sato, Appl. Catal. B-Environ. 123–124 (2012) 9–17.
- [27] S. Laursen, S. Linic, J. Phys. Chem. C 113 (2009) 6689–6693.
- [28] B. Li, H. Cao, J. Mater. Chem. 21 (2011) 3346–3349.
- [29] Q.-P. Luo, X.-Y. Yu, B.-X. Lei, H.-Y. Chen, D.-B. Kuang, C.-Y. Su, J. Phys. Chem. C 116 (2012) 8111–8117.
- [30] K.K. Manga, Y. Zhou, Y. Yan, K.P. Loh, Adv. Funct. Mater. 19 (2009) 3638–3643.
- [31] Q. Xiang, J. Yu, M. Jaroniec, J. Am. Chem. Soc. 134 (2012) 6575–6578.
- [32] T. Xu, L. Zhang, H. Cheng, Y. Zhu, Appl. Catal. B-Environ. 101 (2011) 382–387.
- [33] H.Y. Yang, S.F. Yu, S.P. Lau, X. Zhang, D.D. Sun, G. Jun, Small 5 (2009) 2260–2264.
- [34] N. Yang, J. Zhai, D. Wang, Y. Chen, L. Jiang, ACS Nano 4 (2010) 887–894.
- [35] Z. Zhan, L. Zheng, Y. Pan, G. Sun, L. Li, J. Mater. Chem. 22 (2012) 2589–2595.
- [36] H. Zhang, X. Lv, Y. Li, Y. Wang, J. Li, ACS Nano 4 (2009) 380–386.
- [37] Q. Zhang, C. Tian, A. Wu, T. Tan, L. Sun, L. Wang, H. Fu, J. Mater. Chem. 22 (2012) 11778–11784.
- [38] X.-Y. Zhang, H.-P. Li, X.-L. Cui, Y. Lin, J. Mater. Chem. 20 (2010) 2801–2806.
- [39] Y.H. Ng, A. Iwase, A. Kudo, R. Amal, J. Phys. Chem. Lett. 1 (2010) 2607–2612.
- [40] P. Wang, J. Wang, X. Wang, H. Yu, J. Yu, M. Lei, Y. Wang, Appl. Catal. B-Environ. 132–133 (2013) 452–459.
- [41] H. Yu, R. Liu, X. Wang, P. Wang, J. Yu, Appl. Catal. B-Environ. 111–112 (2012) 326–333.
- [42] A.H. Castro Neto, F. Guinea, N.M.R. Peres, K.S. Novoselov, A.K. Geim, Rev. Mod. Phys. 81 (2009) 109–162.
- [43] Y. Yang, L. Ren, C. Zhang, S. Huang, T. Liu, ACS Appl. Mater. Interfaces 3 (2011) 2779–2785.
- [44] O. Akhavan, ACS Nano 4 (2010) 4174–4180.
- [45] X. Liu, L. Pan, T. Lv, T. Lu, G. Zhu, Z. Sun, C. Sun, Catal. Sci. Technol. 1 (2011) 1189–1193.

- [46] J. Tian, S. Liu, H. Li, L. Wang, Y. Zhang, Y. Luo, A.M. Asiri, A.O. Al-Youbi, X. Sun, RSC Adv. 2 (2012) 1318–1321.
- [47] G. Williams, P.V. Kamat, Langmuir 25 (2009) 13869–13873.
- [48] G. Williams, B. Seger, P.V. Kamat, ACS Nano 2 (2008) 1487–1491.
- [49] S. Wu, Z. Yin, Q. He, X. Huang, X. Zhou, H. Zhang, J. Phys. Chem. C 114 (2010) 11816–11821.
- [50] J.X. Wang, X.W. Sun, Y. Yang, K.K.A. Kyaw, X.Y. Huang, J.Z. Yin, J. Wei, H.V. Demir, Nanotechnology 22 (2011) 325704.
- [51] N.I. Kovtyukhova, P.J. Ollivier, B.R. Martin, T.E. Mallouk, S.A. Chizhik, E.V. Buzaneva, A.D. Gorchinskiy, Chem. Mater. 11 (1999) 771–778.
- [52] R. Jin, W. Gao, J. Chen, H. Zeng, F. Zhang, Z. Liu, N. Guan, J. Photochem. Photobiol. A-Chem. 162 (2004) 585–590.
- [53] W. Wang, L. Zhang, T. An, G. Li, H.-Y. Yip, P.-K. Wong, Appl. Catal. B-Environ. 108–109 (2011) 108–116.
- [54] P. Pichat, C. Guillard, L. Amalric, A.-C. Renard, O. Plaidy, Sol. Energy Mater. Sol. Cells 38 (1995) 391–399.
- [55] A. Nandi, I. Chatterjee, J. Biosci. 11 (1987) 435–441.
- [56] E. Rauwel, A. Galeckas, P. Rauwel, M.F. Sunding, H. Fjellvåg, J. Phys. Chem. C 115 (2011) 25227–25233.
- [57] R.M. Sheetz, I. Ponomareva, E. Richter, A.N. Andriotis, M. Menon, Phys. Rev. B 80 (2009) 195314.
- [58] Y. Xu, K. Sheng, C. Li, G. Shi, ACS Nano 4 (2010) 4324–4330.
- [59] M. Chen, X. Wang, Y.H. Yu, Z.L. Pei, X.D. Bai, C. Sun, R.F. Huang, L.S. Wen, Appl. Surf. Sci. 158 (2000) 134–140.
- [60] B. Jiang, C. Tian, Q. Pan, Z. Jiang, J.-Q. Wang, W. Yan, H. Fu, J. Phys. Chem. C 115 (2011) 23718–23725.
- [61] A.B. Djurišić, W.C.H. Choy, V.A.L. Roy, Y.H. Leung, C.Y. Kwong, K.W. Cheah, T.K. Gundu Rao, W.K. Chan, H. Fei Lui, C. Surya, Adv. Funct. Mater. 14 (2004) 856–864.
- [62] K. Hoffmann, D. Hahn, Phys. Status Solidi A-Appl. Mater. 24 (1974) 637–648.
- [63] A. Pöppel, G. Völkel, Phys. Status Solidi A-Appl. Mater. 121 (1990) 195–204.
- [64] S. Moribe, T. Ikoma, K. Akiyama, Q. Zhang, F. Saito, S. Tero-Kubota, Chem. Phys. Lett. 436 (2007) 373–377.
- [65] C.H. Geisler, G.L. Simmons, Phys. Lett. 11 (1964) 111–112.
- [66] R.B. Lal, G.M. Arnett, J. Phys. Soc. Jpn. 21 (1966) 2734–2735.
- [67] K. Vanheusden, C.H. Seager, W.L. Warren, D.R. Tallant, J. Caruso, M.J. Hampden-Smith, T.T. Kodas, J. Lumines. 75 (1997) 11–16.
- [68] K. Vanheusden, W.L. Warren, C.H. Seager, D.R. Tallant, J.A. Voigt, B.E. Gnade, J. Appl. Phys. 79 (1996) 7983–7990.
- [69] K.A. Müller, J. Schneider, Phys. Lett. 4 (1963) 288–291.
- [70] H. Zhou, A. Hofstaetter, D.M. Hofmann, B.K. Meyer, Microelectron. Eng. 66 (2003) 59–64.
- [71] N.Y. Garces, N.C. Giles, L.E. Halliburton, G. Cantwell, D.B. Eason, D.C. Reynolds, D.C. Look, Appl. Phys. Lett. 80 (2002) 1334–1336.
- [72] W.K. Liu, K.M. Whitaker, A.L. Smith, K.R. Kittilstved, B.H. Robinson, D.R. Gamelin, Phys. Rev. Lett. 98 (2007) 186804.
- [73] K.M. Whitaker, S.T. Ochsenbein, V.Z. Polinger, D.R. Gamelin, J. Phys. Chem. C 112 (2008) 14331–14335.
- [74] D. Galland, A. Hervé, Phys. Lett. A 33 (1970) 1–2.
- [75] A. Janotti, C.G. Van de Walle, Phys. Rev. B 76 (2007) 165202.
- [76] M. Zhu, P. Chen, M. Liu, J. Mater. Chem. 22 (2012) 21487–21494.
- [77] Y. Zhang, Z.-R. Tang, X. Fu, Y.-J. Xu, ACS Nano 4 (2010) 7303–7314.
- [78] T.-Y. Ke, C.-Y. Lee, H.-T. Chiu, Appl. Catal. A-Gen. 381 (2010) 109–113.